THE ASTROPHYSICAL JOURNAL, 425:755–766, 1994 April 20

HOT GAS AND THE ORIGIN OF THE NEBULAR CONTINUUM IN NOVAE

PEDRO SAIZAR
Department of Astronomy and Astrophysics, University of Pennsylvania, Philadelphia, PA 19104
AND
GARY J. FERLAND
Department of Physics and Astronomy, University of Kentucky, Lexington, KY 40506
Received 1993 August 23; accepted 1993 October 22

ABSTRACT

A featureless blue continuum (with constant f_ν) is a defining feature of declining classical novae. The fact that f_ν is constant into the infrared, and the absence of a Balmer jump, suggests that this continuum originates in hot tenuous gas. The electron temperature and density of the hot gas phase of classical nova QU Vul 1984 are estimated from ground-based optical and *IUE* ultraviolet observations. This region has a temperature of 10^5–10^6 K, and a density in the range of 2×10^4 to 3×10^5 cm^{-3}. In addition, a colder, denser shell composed of many "clumps" or condensations is present, and it is responsible for most of the optical-to-ultraviolet emission lines. The hot gas, however, may be much more massive and could dominate the energetics of the ejecta. The total returned mass could be as high as 10^{-4} and 4×10^{-3} $M_\odot$, depending on conditions in the hot gas.

The large mass of the shell, in combination with the high metallicity found in this nova, supports the idea that novae may be an important contributor to the chemical enrichment of the interstellar medium.

Subject headings: circumstellar matter — ISM: abundances — novae, cataclysmic variables — stars: individual (QU Vulpeculae) — ultraviolet: stars

1. INTRODUCTION

The violence of a classical nova outburst invariably leads to the ejection of matter into the surrounding interstellar space. According to the accepted model for classical nova outbursts (see, e.g., Starrfield 1989, and references therein), the ejected shell's chemical composition is enriched in part via nucleosynthesis during the outburst and also by chemical mixing with the underlying white dwarf. Thus, studies of the mass content and chemical abundances in nova ejecta can be of importance to studies of chemical evolution of the Galaxy as well as to the physics of nova outbursts.

Unfortunately, astronomers can rarely resolve nova shells, as they tend to occur at great distances and cannot rival supernovae in extent and luminosity. The structure of most nova shells must, therefore, be deduced from the observed emission. In this sense, much effort has been invested in studying the emission line spectra that are observed during the postoutburst decay. A major comparative optical study has been recently published by Williams et al. (1991), while a review of ultraviolet observations of novae can be found in Starrfield (1990).

Postoutburst optical spectra are usually dominated by forbidden transitions from low and medium ionization stages of common elements. This "nebular" phase of ionization is believed to be produced in a warm ($T_e \sim 10^4$ K), clumpy shell. However, in their study of the infrared spectrum of nova V1500 Cygni, Grasdalen & Joyce (1976) identified several emission lines as being produced by highly ionized species, such as those observed in the solar corona. They then put forward the novel concept that this emission could be produced in a physically distinct region within the nova shell, at a much higher temperature than the region producing all the other low- and medium-ionization species. Ferland, Lambert, & Woodman (1977), and Shields & Ferland (1978), showed that the coronal emission was also present in the optical spectra, in transitions such as [Fe X] λ6374. These lines are often hidden in the wings of much brighter lines, which are broadened by the relatively large expansion velocities of the shell.

The concept of a "coronal line region" was challenged by Williams et al. (1991), who argued that a very hot remnant could produce the observed ionization levels by means of simple photoionization. Indeed, there is considerable evidence that postoutburst novae undergo a period of relatively constant bolometric luminosity, usually near the Eddington limit (Starrfield 1989 described the processes leading to and following a nova outburst). During this time, the underlying white dwarf decreases in radius back to its preoutburst size, and thus its temperature may increase up to several hundred thousand degrees. Additional evidence on the production of coronal emission via photoionization was provided by Saizar et al. (1991), for the case of Nova PW Vulpeculae 1984. Attending the fact that the coronal emission was only transient, Williams et al. (1991) proposed a model that included a "coronal line" stage for the evolution of nova shells. Here, the high ionization lines are produced at the illuminated face of the dense clumps which also produce the "nebular" emission lines (i.e., O III], etc.).

There is, however, additional evidence suggesting the presence of gas at very high temperature in nova shells. Gallagher & Ney (1976) showed that the optical-to-IR continuum of a declining nova was dominated by free-free emission. The absence of a Balmer jump shows that the gas producing the free-free emission must be hot. Following this, Ferland, Lambert, & Woodman (1986) showed that the continuum spectrum of Nova V1500 Cygni could not be explained by a gas at a temperature that is derived from lower ionization lines. Nebular diagnostic techniques, using emission lines such as the well-known optical [O III] transitions, would yield electron temperatures of the order of 10,000 K. The continuum produc-

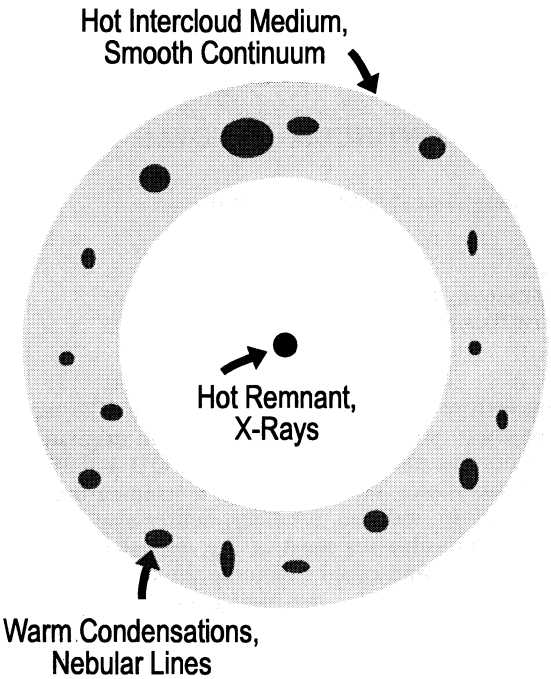

FIG. 1.—Composite model of a nova shell. The ejecta consists of warm ($T \sim 10^4$ K), dense clouds embedded in a hot ($T \sim 10^6$ K), tenuous gas. Both phases are photoionized by the hard white dwarf continuum. The warm phase is further photoionized by the free-free continuum generated in the hot gas.

ed by gas at this temperature was too weak compared to the observed continuum. Saizar et al. (1992, hereafter S92), reached the same conclusion for Nova QU Vul 1984 and pointed out that, in addition to a strong continuum level, a very weak hydrogen Balmer jump also indicates a high temperature. An estimate of the relative intensities of the hot and warm continua revealed that the hot continuum may dominate both the mass content and the energetics of the ejected shell.

In this paper, we propose a model for the ejecta that attempts to explain both the line and continuum emission. This two-phase model consists of a "warm" ($T_e \sim 10^4$ K), high-density clumpy shell which is photoionized by a background composed of both the continuum of the remnant as well as from the "hot" ($\sim 10^5$–10^6 K), tenuous gas (Fig. 1). In this picture, high-energy photons from the underlying white dwarf are partially reprocessed into ultraviolet photons via interactions in the hot gas. This reprocessed radiation is then capable of producing the observed transitions in the warm condensations via photoionization. A refinement of this idea, including shadowing effects due to the high-density clumps, has been recently given by Williams (1992).

In § 2, we present the methods used to constrain the physical conditions of the hot gas. We then proceed to examine in detail Nova QU Vul 1984. Section 3 describes some of the previous results on this object. In §§ 4 and 5 we compare theoretical predictions from nebular physics with the observations in order to derive parameters such as the electron temperature and density, mass, geometry, and energetics of the ejecta. A summary and a discussion on the implication of these findings for galactic nucleosynthesis studies closes this paper.

2. PHYSICAL CONDITIONS IN THE HOT GAS

In this section we discuss the methods that will allow us to set limits to the electron temperature and density of the hot gas. To this end, we will derive some expressions which will be useful in comparing the observed continuous spectrum with the theoretical predictions. In what follows, we will consider a two-phase gas which is photoionized by a blackbody, the emergent continuum from the remnant. We will assume that the physical conditions in the warm "nebular" phase have been determined from nebular line diagnostics, so that this contribution can be easily removed from the observed spectrum (as mentioned in § 3, the uncertainty in the warm temperature is usually much smaller than any other errors involved). The remaining fluxes, then, correspond to the hot gas emission. The theoretical emissivities from hydrogen and helium have been calculated by Ferland (1980, hereafter F80), for a wide range of temperatures.

2.1. *Temperature of the Hot Gas*

The temperature of the gas can be measured from the depth of the observed Balmer jump, which is an inverse function of this parameter.

The shape of the observed continuum can be expressed as the sum of the contributions by the warm and the hot phases. There is also an additional contribution from the white dwarf, which we will neglect for now, since little of its emission is expected to appear in the region near the Balmer jump (see S92). Therefore, the total flux of the observed UV-optical-IR continuum, vf_ν, relative to the line flux of Hβ, is given by

$$\left.\frac{vf_\nu}{f_{H\beta}}\right|_{obs} \sim \left.\frac{v\gamma_\nu}{4\pi j_{H\beta}}\right|_{warm} + \frac{E_{hot}\, v\gamma_\nu(\mathrm{hot})}{E_{warm}\, 4\pi j_{H\beta}(\mathrm{warm})}, \quad (1)$$

where $v\gamma_\nu$ and $4\pi j_{H\beta}$ are the emission coefficients of the continuum and Hβ, respectively, in ergs cm^3 s^{-1}, and $E = N_e N_+ V$, is the emission measure for each gas phase, where V is the volume. In this equation, we have assumed that all of the Hβ flux is produced in the warm phase, which may introduce errors as large as 50%. We further discuss this assumption below.

If the electron temperature in the warm phase can be found from the emission-line diagnostics, then the above equation can be used to subtract the warm phase from the observed spectrum, and then the hot spectrum can be examined.

The Balmer continuum in nebular shells, produced by hydrogen recombination, weakens relative to Hβ as the temperature increases. The Balmer jump itself is difficult to measure as it is out of range of the *IUE* spectra and often of the optical spectra. In addition, there are relatively few portions of any spectra free from line contamination. Thus, we chose to measure the strength of the Balmer jump as the ratio vf_ν(3500 Å)/vf_ν(4100 Å). This ratio is shown in Figure 2, from data given by F80. The observed ratio, once the warm phase has been substracted, can be used to set a lower limit to the temperature of the hot gas. This is only a lower limit, since the gas may be hotter and the observed "jump" mostly noise.

An independent lower limit to the temperature of the hot gas can be obtained from the observed emission from Hβ. The strength of the Balmer lines is a decreasing function of temperature for a given emission measure (Osterbrock 1989). Thus, although some Hβ flux can be produced by the hot phase, most of it is expected to come from the warm gas. At its lowest temperature, the hot gas cannot produce more than half of the line emission (equivalently, for the warm gas at its highest temperature).

In order to eliminate the density dependence on the fluxes, we need to find a suitable additional flux. The continuous

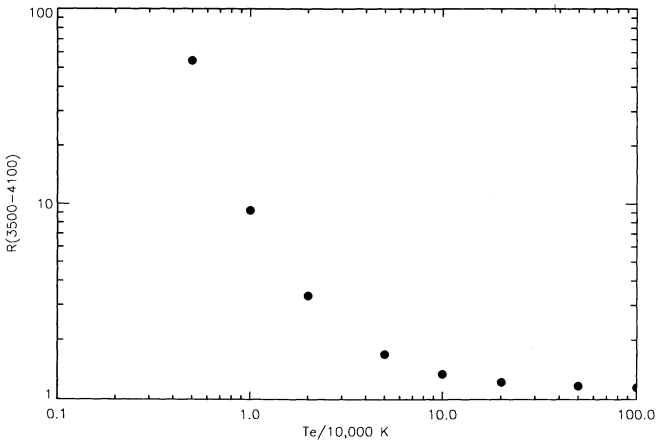

FIG. 2.—Depth of the Balmer jump, $v\gamma_\nu(\lambda3500)/v\gamma_\nu(\lambda4100)$, as a function of temperature (data from Ferland 1980).

emission in the far-UV continuum is also sensitive to temperature, but it has the opposite dependence to Hβ. The ratio can therefore be expected to be a sensitive temperature indicator. In addition, the far UV continuum from the warm gas can be safely neglected. Thus, choosing a continuum point at 1500 Å, we obtain

$$\left.\frac{v\gamma_\nu(1500\text{ Å})}{4\pi j_{H\beta}}\right|_{obs} = \frac{vf_\nu(1500,\text{ hot}) + vf_\nu(1500,\text{ warm})}{f_{H\beta}(\text{hot}) + f_{H\beta}(\text{warm})} \quad (2)$$

$$= \left.\frac{vf_\nu(1500)}{f_{H\beta}}\right|_{hot} \times \left(1 + \frac{f_{H\beta}(\text{warm})}{f_{H\beta}(\text{hot})}\right)^{-1} . \quad (3)$$

In Figure 3 we show the emissivity of the $\lambda1500$ continuum relative to Hβ as predicted by F80. The minimum temperature of the hot gas corresponds to $f_{H\beta}(\text{hot}) = f_{H\beta}(\text{warm}) = 1/2f_{H\beta}(\text{obs})$. So, a lower limit to the temperature can be obtained by just comparing the predictions to twice the observed ratio.

An upper limit to the temperature can also be obtained. In our model (cf. § 1), the hot gas is assumed to be a tenuous shell in photoionization equilibrium with the white dwarf. Under this condition, the maximum temperature of the gas is the Compton temperature of the radiation field, which is roughly

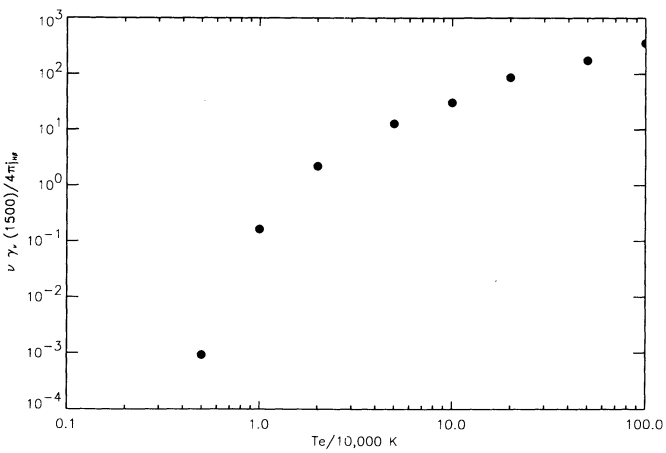

FIG. 3.—Continuum emissivity at $\lambda1500$ relative to the line flux of Hβ, as a function of temperature. Data from Ferland (1980).

the photospheric temperature of the white dwarf. The WD's temperature is known to vary as the outburst progresses. Bath & Shaviv (1976) and Gallagher & Starrfield (1976) showed that the white dwarf decreases in radius at constant luminosity, roughly equal to the Eddington luminosity, for several months to years after the outburst. The maximum temperature that the star reaches will be given by its preoutburst radius, as

$$T = 6.12 \times 10^5\ \text{K}\left(\frac{L_{38}}{R_9^2}\right)^{1/4}, \quad (4)$$

where $L_{38} = 10^{-38}L_{Edd}$, $R_9 = 10^{-9}R_{WD}$, L_{Edd} and R_{WD} are the Eddington luminosity and the white dwarf radius, which are taken as 10^{38} ergs s^{-1} and 10^9 cm. These are given as a function of white dwarf mass by Starrfield (1989). For masses above 1 $M_\odot$, L_{38} varies between 1.6 and 2.3, and R_9, between 0.2 and 0.9.

2.2. *The Density of the Hot Gas*

As indicated in § 1, we propose that the hot phase is in photoionization equilibrium with the stellar radiation field. In most instances, the postoutburst white dwarf can be represented as a hot blackbody whose continuum peaks in the extreme UV to X-ray bands (Fig. 1). Therefore, the observed UV continuum should contain a contribution from the underlying blackbody in the form of a Rayleigh-Jeans spectrum. This would be undetected if the white dwarf is hot and the nebula is optically thick to the ionizing radiation. Then the shell would reprocess the majority of the WD luminosity into the UV. In this case, the incident radiation beyond the Lyman-continuum is mostly absorbed via photoelectric absorption and Compton scattering, and reprocessed into an UV/optical free-free spectrum. However, as the electron density decreases, the nebula eventually becomes optically thin to the ionizing photons. The free-free continuum becomes fainter, and the observed UV continuum will resemble that of the white dwarf (see Fig. 4).

One can think of this in terms of the ionization parameter U, which is defined here as the ratio between the photon density

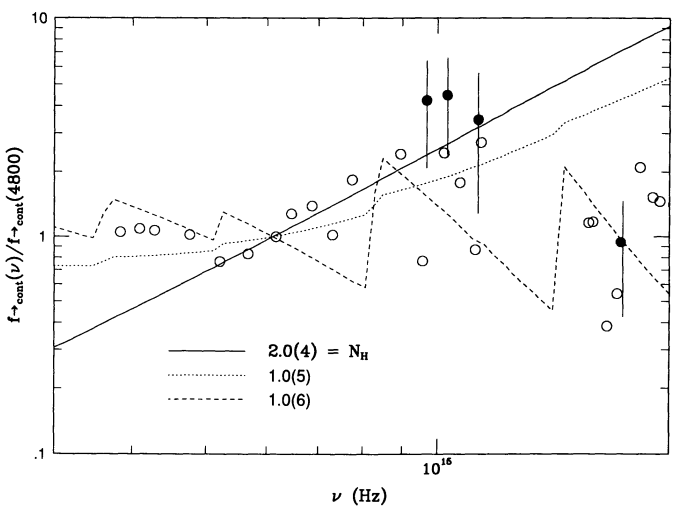

FIG. 4.—The continuous spectrum of QU Vul normalized to the continuum flux at Hβ. *Closed circles:* observed fluxes in regions assumed free of emission lines; *open circles:* fits to the continuum around emission lines. The errors are assumed to be similar for all points. Lines are calculated emergent continua, with densities as indicated. The model parameters are described in the text.

of the ionizing radiation and the electron density (see, e.g., Davidson 1977), i.e.,

$$U = \frac{Q(\mathrm{H})}{4\pi r^2 N_{\mathrm{H}} c}, \quad (5)$$

where $Q(\mathrm{H})$ is the number of ionizing photons per second emitted by the white dwarf, and N_{H} is the hydrogen density at a distance r from the source. For a given continuum shape and chemical composition, the equations of ionization equilibrium uniquely determine the temperature of the gas and the ionization structure. Conversely, if the electron temperature and the ionic concentrations can be estimated from emission-line diagnostics, the electron density can be constrained by setting limits on the possible ionizing continua.

In order to carry out these calculations we constructed a series of photoionization models using the radiative-collisional equilibrium code CLOUDY (Ferland 1993). Basically, this code solves the ionization and heating-cooling equilibrium equations for a shell of a specified geometry. The other input parameters relate to the shape and luminosity of the ionizing spectrum, the chemical composition of the gas, and the radius of the shell. The code then predicts the emergent spectrum for both lines and continuum.

We chose the fluxes at $\lambda\lambda$1500 and 4800, since they are relatively free from line contamination. The observed ratio $f_\nu(1500)/f_\nu(4800)$ is then predicted by CLOUDY for a wide range of gas densities and stellar temperatures (in essence, for a range of U's). An upper limit for the stellar temperature of $\sim 10^6$ K has been obtained in the previous section. For the observed continuum to contain a contribution from a hot white dwarf, the free-free emission should be faint, and therefore, the gas should be tenuous. This procedure, then, gives us a lower limit to the density. This is illustrated in Figure 4, for the case of nova QU Vul 1984. The solid curves represent emergent continua for three different densities, and the dots are the observed continuum fluxes. The actual calculations are presented in § 2.

An upper limit to the density can be obtained from the observed flux of Hβ. As mentioned in the previous subsection, this line may be produced in different amounts by both phases. But, even if a single phase was present, the predicted flux can never be larger than the observed one, thus effectively yielding an upper limit for the electron density for a given temperature of the radiation field.

Before analyzing the multiwavelength spectra of QU Vul, let us briefly review some of the work previously done on this object.

3. OVERVIEW OF PREVIOUS WORK

In S92, we used ground-based optical and satellite ultraviolet spectra to study the physical conditions in the expanding shell of Nova QU Vul. A few useful numbers concerning this object are summarized in Table 1, taken from S92.

The reddening toward the nova has been obtained by comparing the observed and the theoretical ratio He II λ4686/He II λ1640 (Seaton 1978). The results indicate that $E(B-V) = 0.61 \pm 0.10$. This is also confirmed by one observation of the 2200 Å feature due to interstellar reddening. The distance was then deduced from the luminosity–"speed class" relationship (Warner 1989) to be 3.0 ± 1.0 kpc.

Using various optical and UV emission-line fluxes, we derived temperatures in the warm gas phase of $T_e = (1.0 \pm 0.08) \times 10^4$ K. The electron density maintained a remarkably constant level of $N_e \sim 10^7$ cm^{-3}, for the period 126–500 days, and declined at later dates. Since nova shells are expected to show declining densities as they expand, we have suggested (S92) that this constancy is evidence for continuous mass loss, although other mechanisms, such as magnetic confinement, might play a role. There is no evidence, however, that QU Vul has a magnetic white dwarf.

TABLE 1

QU VULPECULAE: SOME USEFUL NUMBERS

Parameter	Value
Date of maximum	1984 Dec 25
m_V (maximum) (mag)	+5.6
t_3 (days)	40
$E(B-V)$	0.61 ± 0.10
b (galactic latitude)	−6°
Distance (kpc)	3.0
M_V	-8.0 ± 0.9

Abundances were also obtained from diagnostic line ratios by selecting pairs of lines with similar ionization potential ranges in order to minimize fluctuations due to inhomogeneities in the shell. The average abundances by number in terms of the solar composition are [He/H] = 5, [C/H] = 0.8, [N/H] = 44, [O/H] = 10, [Ne/H] = 60, [Mg/H] = 6, [Al/H] = 90, [Si/H] = 2, and [Ar/H] = 0.7. These abundances are averages from the ones obtained by various methods by us (S92) and Greenhouse et al. (1988). These results are in qualitative agreement with hydrodynamic models of slow ONeMg white dwarfs (Starrfield, Sparks, & Truran 1986). The high abundance of helium might support the idea of continuous hydrogen burning past the peak of the outburst. The secondary star, normally an unevolved red dwarf, is expected to have a helium abundance close to accepted cosmic values.

The continuous spectrum was measured by substracting the emission-line fluxes, and also by looking at the few regions with no lines present. Although weak, continuous fluxes were observed up to about 2 years after the outburst. Ultraviolet, optical and infrared data (as described in S92), were joined to give the broadest possible picture. The continuum has a flat (i.e., $f_\nu \sim$ constant) featureless appearance at most observed days, which strongly suggests that the shell contains gas at a high temperature (Gallagher & Ney 1976).

4. THE SHELL OF QU VULPECULAE

4.1. *Electron Temperature and Density*

First, let us apply equation (1) in order to constrain the temperature from the depth of the Balmer jump. In order to subtract the warm phase from the observed spectrum, we have averaged portions of the data at day 554 about the wavelengths listed by F80. In Table 2, we list these average fluxes relative to Hβ, in dimensionless units. In the third column, we include the predicted relative continuum emission coefficient for a mixture of 50% hydrogen and 50% helium, at $T = 10^4$ K (cf. § 3). The subtracted spectrum, shown in the last column, indicates that the Balmer jump is virtually absent. The depth of the Balmer jump, which we measure as the ratio $\nu f_\nu(3500)/\nu f_\nu(4100)$, is shown as a function of temperature in Figure 2. Theoretical values for the Balmer jump are given in Table 3, based on F80. From this figure and the observed depth inferred from Table 2, we estimate a lower limit for $T_e \sim 1.7 \times 10^5$ K.

TABLE 2

CONTINUOUS SPECTRUM OF QU VULPECULAE

	$vL_v/L_{H\beta}$		
λ (1)	Observed (2)	Cold (3)	Hot (4)
1500.....	30.0	0.3	29.7
1800.....	19.1	1.5	17.6
2500.....	21.4	3.3	18.1
3300.....	19.1	12.6	6.5
3500.....	18.8	12.6	6.2
4100.....	10.9	5.5	5.4
4700.....	7.6	2.9	4.7
5400.....	4.6	4.3	~0
6800.....	4.9	6.1	~0

The second method is based on the relative contributions of Hβ to each phase (cf. eq. [3].) From Table 3, we see that the observed continuum-to-line ratio, $vf_v(1500)/f_{H\beta} \sim 30$. At its minimum temperature, half of the Hβ emission is produced by the hot gas, and therefore, the above ratio produced by the hot gas alone is equal to 60. In Figure 3, we show this continuum-to-line ratio, as predicted by F80, for a mixture of hydrogen and helium at various temperatures. A ratio of 60 implies that the minimum temperature of the hot phase is near 10^5 K, which is in good agreement with our previous estimate.

Finally, we can find the maximum gas temperature from equation (4). For a 1 $M_\odot$ star, the temperature is of the order of 9×10^5 K, and it increases by about a factor of 2 for a 1.4 $M_\odot$ white dwarf.

In order to set limits on the density, as explained in § 2, we need to construct a grid of photoionization models for various ionization parameters and an assumed chemical composition. Fortunately, thanks to previous work done on this nova, we can avoid simple but probably unrealistic models, such as parallel-plane geometries.

The radiation field incident on the inner face of the shell can be approximated as a blackbody of less than 10^6 K. In fact, X-ray observations suggest that the white dwarf is at a temperature of about 3×10^5 K (Ögelman, Krautter, & Beuermann 1987). The authors caution, however, that the error may be large, so we will use this only as a guide for our study.

The luminosity of a postoutburst white dwarf is expected to be close to the Eddington limit until the so-called turnoff time of the nova, so we will adopt a luminosity of $L_{Edd} = 2 \times 10^{38}$ ergs s^{-1}.

The chemical composition has been obtained by S92 for the warm phase. We will assume the same chemical composition for the hot phase, since it is reasonable to expect that the chemically rich ejecta from the white dwarf is involved. We also adopted a spherical geometry for the hot gas, with an outer radius given by the expansion velocities listed in Table 1, $R \sim 7 \times 10^{15}$ cm. A radio study by Taylor et al. (1987) shows that the shell is not spherical, but since we are attempting only to set limits, we will neglect for now this deviation.

TABLE 3

EMISSION FROM THE HOT PHASE

$T(\times 10^4$ K)	$\gamma(3646+)/\gamma(3646-)$	$v\gamma_v^{hot}(1500)/I_{H\beta}^{hot}$
1.....	18.10	1.00
2.....	4.57	5.30
5.....	1.79	23.2
10.....	1.30	52.3
20.....	1.11	144.
50.....	1.04	288.
100.....	1.02	589.

TABLE 4

OBSERVED FLUXES FOR CONTINUUM DIAGNOSTICS

$t - t_0$	$I(H\beta)$	$f_\lambda(1500)$	$f_\lambda(4861)$	$vf_v(1500)/I_{H\beta}$[a]	$vf_v(4861)/I_{H\beta}$[a]
158....	6.75(−11)	7.56(−14)	9.36(−14)	39.13	6.76
182....	6.40(−11)	1.11(−13)	8.86(−14)	60.63	6.71
191....	6.27(−11)	6.72(−14)	8.67(−14)	37.50	6.71
204....	6.08(−11)	5.18(−14)	8.40(−14)	29.75	6.71
309....	3.41(−11)	1.04(−14)	5.39(−14)	10.66	7.68
340....	2.99(−11)	2.09(−14)	4.69(−14)	24.50	7.63
462....	1.61(−11)	1.12(−14)	2.08(−14)	24.38	6.27
554....	1.12(−11)	6.34(−15)	1.51(−14)	19.75	6.56
627....	7.98(−12)	3.00(−15)	1.34(−14)	13.13	8.17

[a] Corrected for reddening.

In Figure 4, we show the predicted emergent spectrum for various hydrogen densities, and for a blackbody temperature $T_{BB} = 5 \times 10^5$ K. Note that the scale is normalized to the continuum near Hβ. We can see that the density must lie in the range 2×10^4–10^6 cm^{-3} to fit the continuum. At higher densities, the gas becomes too cool because of the decreasing ionization parameter. This produces a UV continuum which is too weak and a Balmer jump which is too strong.

Another indication of the point at which the warm gas becomes too warm due to a high electron density is given by the luminosity of Hβ predicted by our models. The observed luminosity for day 554 is $L_{H\beta} \sim 8 \times 10^{33}$ ergs s^{-1}. In the example discussed above, with $T_{BB} \sim 5 \times 10^5$ K, models with electron densities larger than $\sim 4 \times 10^5$ cm^{-3} predict Hβ luminosities larger than observed, because a larger fraction of cooler gas produces recombination lines rather than free-free emission.

Next, we repeat this procedure for a number of models, varying both the blackbody temperature and the hydrogen density of the gas. In Table 4, we list the observed line intensity of Hβ, and the continuum fluxes at 1500 and 4861 Å, respectively. In the last two columns, we list the continuum fluxes relative to Hβ, in dimensionless units and corrected for reddening. Before using them, however, we need to substract the warm gas phase. From F80's tables, we obtain $v\gamma_v(1500)/4\pi j_{H\beta} = 0.30$, and $v\gamma_v(4861)/4\pi j_{H\beta} = 1.80$, for gas at $T = 10^4$ K. The resulting fluxes are listed in Table 5. The last column shows the continuum flux ratio, which we will use to constrain the density.

The photoionization code CLOUDY has been used with the parameters described above in order to find the relationship

TABLE 5

EMISSION FROM THE HOT GAS PHASE

$t - t_0$	$vf_v(1500)/I_{H\beta}$	$vf_v(4861)/I_{H\beta}$	$vf_v(1500)/vf_v(4861)$
158.....	39.0	4.96	7.9
182.....	60.4	4.91	12.3
191.....	37.3	4.91	7.6
204.....	29.6	4.91	6.0
309.....	10.5	5.88	1.8
340.....	24.3	5.83	4.2
462.....	24.1	4.47	5.4
554.....	19.6	4.76	4.1
627.....	13.0	6.37	2.0

between our continuum flux ratio and the electron density. This is plotted in Figure 3. The dotted lines are the model predictions for various temperatures of the white dwarf as indicated. Note that as the density decreases, the ionization parameter increases, and as the temperature increases, the slope of the continuum raises, as expected. The vertical solid lines delimit the area for which the line luminosity of Hβ is greater than the value shown. To the right of the isoluminosity curve labeled "34," the Hβ luminosity is greater than observed, and, therefore, these densities are considered to unlikely represent the actual conditions in the gas. In order to evaluate the errors due to the poorly determined distance, an additional boundary line has been added which corresponds to an order of magnitude increase in the luminosity of Hβ. Note also that this still corresponds to lower densities than the warm gas phase. Finally, the middle horizontal solid line indicates the observed ratio for day 554, and the remaining solid lines are the upper and lower limits given by the observational errors. They have been obtained by setting limits to the noise in a spectral region assumed to be free from line contamination. From the graph, we obtain a range of densities of 2×10^4 to 3×10^5 cm^{-3}. This is substantially lower than the density of the warm gas phase, and even if the distance was underestimated by as much as a factor of 3, the hot gas would still be one order of magnitude less dense than the warm gas.

To summarize, the shape of the continuum spectrum suggests that the gas has a temperature $T_{\rm hot} \sim 10^5$–10^6 K. The photoionization simulations show that this is produced if the gas is in equilibrium with the radiation field of the white dwarf, and has a density in the neighborhood of $N_{\rm e,hot} \sim 2 \times 10^4$–$3 \times 10^5$ cm^{-3}. These results can now be used to set limits on other parameters.

TABLE 6

MODEL PARAMETERS AND PREDICTIONS

STAR $T_{\rm BB}$	EJECTA $N_{\rm H}$	T_e	$N_{\rm H}T$	$M_{\rm H}/M_{\rm C}$	$\epsilon_{\rm cold}$
		Hot Gas Phase			
1.0(6).....	2.0(4)	3.8(5)	8(9)	920	2.2(−6)
	3.0(4)	3.0(5)	9(9)	548	5.5(−6)
	5.0(4)	2.5(5)	1(10)	300	1.7(−5)
5.0(5).....	6.0(4)	7.0(4)	4(9)	132	4.5(−5)
	8.5(4)	6.3(4)	5(9)	89	9.6(−5)
	1.4(5)	5.4(4)	8(9)	50	2.8(−4)
2(5).....	2.0(5)	2.2(4)	4(9)	22	9.0(−4)
	3.0(5)	3.1(4)	9(9)	18	1.7(−3)
		Cold Gas Phase			
... .	1.0(7)	1.0(4)	1(11)	1	...

5. THE OVERALL SHELL STRUCTURE

In this section, we combine the results obtained for the density and temperature, in order to derive additional properties of the shell, such as the mass, geometry, and energetics.

Since the hot gas has been poorly constrained, we need to derive the additional parameters for a grid of possible hot gas phases, and then examine which models offer more reasonable solutions.

In Table 6, we list the parameters adopted for our grid of photoionization models. Each entry, under "hot gas phase," corresponds to one point within the gray area in Figure 5, so

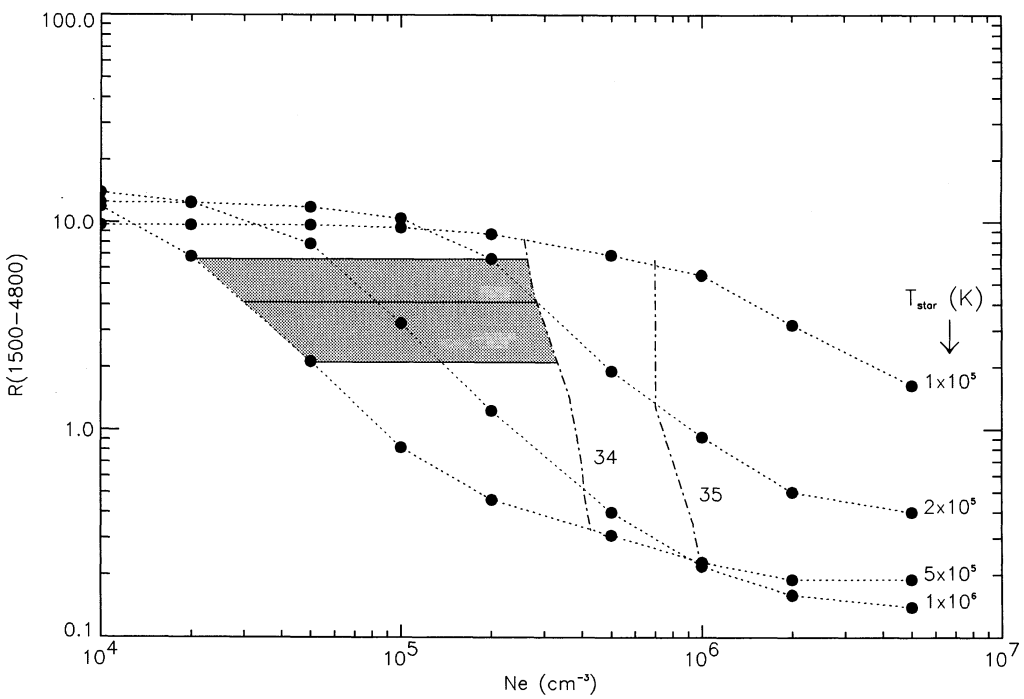

FIG. 5.—Density diagnostics. *Dotted lines:* model predictions of the UV/optical continuum slope for various stellar temperatures. The large filled dots are the models actually run. *Solid lines:* observed flux ratio, and its upper and lower limits. The shaded area delimits the range of densities which are consistent with the observations. *Dot-dashed lines:* Hβ isoluminosity curves. The "34" label corresponds to log L(Hβ) = 10^{34} ergs s^{-1}.

these are our acceptable models for the hot gas. The last entry shows the values for the warm gas phase. The first two columns show the white dwarf temperature and the gas density adopted as input data for the photoionization models. The next column lists the predicted average electron temperature in the shell. The mass ratio of both gas phases and the filling factors, listed in the remaining columns, are discussed in the following sections.

The model parameters used for these calculations are as follows: inner shell radius, $R_i = 10^{15}$ cm; outer radius, $R_o = 7 \times 10^{15}$ cm; white dwarf luminosity, $L_{BB} = 2 \times 10^{38}$ ergs s^{-1}; and spherical geometry for the hot gas. The abundances are the same as discussed in § 3. The remaining input parameters, the white dwarf temperature, and the shell's hydrogen density, are to be varied in our grid, and are those listed in the first two columns of Table 6.

5.1. *The Mass of the Ejecta*

The procedure to estimate the mass from the level of the continuum was discussed in our earlier paper on QU Vul (S92). With these new estimates of the electron density, we can now reevaluate the ejected masses in both gas phases.

In that paper, an expression for the nebular-to-coronal mass ratio was derived from the ratios of emission measures. Assuming that $E \sim N_e^2 V \sim N_e M$, where V and M are the volume and the mass of the emitting region, we obtained

$$\frac{M_{cor}}{M_{neb}} = 3 \times \frac{N_{neb}}{N_{cor}} t_{cor}^{0.5} . \quad (6)$$

From the temperatures and densities derived in the previous sections it follows that the coronal line region has a mass between 18 and 900 times the nebular mass, as shown in Table 6. In S92, we also found the individual masses from the luminosity of Hβ, by assuming that all of this line is produced in the nebular region, which again introduces an error not larger than a factor of 2. The constraints on the density and temperature in the ejecta imply that the total mass of the ejecta lies in the range 1.0×10^{-4} to 4.5×10^{-3} $M_\odot$. Based on an analysis of high-ionization infrared lines, Greenhouse et al. (1988) obtained a lower limit to the coronal mass of $M > 9 \times 10^{-4} M_\odot$.

5.2. *Evidence for Pressure Equilibrium*

The fact that the densities of the hot and warm phases are different suggests that they might be in pressure equilibrium, i.e.,

$$(N_e kT_e)_{hot} = (N_e kT_e)_{warm} . \quad (7)$$

In § 4, we showed that the hot gas density has a range of values between 2×10^4 and 3×10^5 cm^{-3}. These values were obtained from Figure 5 for a variety of stellar temperatures and for a specific geometry and chemical composition in the gas. The photoionization models used to predict the relationship between the continuum color and density also give us the average temperature in the gas, which we need to evaluate the pressure.

In Table 6 we show the gas pressure for several models that lie within the shadowed area in Figure 5. The pressure of the hot gas is roughly one order of magnitude lower than the pressure of the warm gas, shown in the last line of Table 6. This suggests that the two phases are not in pressure equilibrium. Given the large uncertainties, this may not be a conclusive indication that the gas is not in pressure equilibrium. It is possible that pressure equilibrium occurs at some point within the shell, since the electron temperature varies with radius and we have also made the simplifying assumption of constant density for both phases. Naturally, there is no compelling reason to demand pressure equilibrium as both phases may be only loosely associated.

5.3. *Evidence for a "Clumpy" Structure*

The assumption of spherical geometry for the hot gas is in part inspired from the appearance of supernova shells. The Crab Nebula, for instance, shows bright filaments of gas embedded in a diffuse shell. In the model we envision, the hot intercloud medium fully fills its volume, and covers the continuum source. Williams (1992) discusses the effect on the ionization structure of clumps embedded in a hotter intercloud medium, including the effect of shadowing by the clumps.

The ratio of emission measures of both phases is given by

$$\frac{E(\text{hot})}{E(\text{warm})} = \frac{N_e^2(\text{hot})V(\text{hot})}{N_e^2(\text{warm})V(\text{warm})} \sim \frac{1}{\epsilon} \frac{N_e^2(\text{hot})}{N_e^2(\text{warm})} \quad (8)$$

$$= 3t_{hot}^{0.5} \quad (9)$$

where ϵ is the filling factor of the warm gas, and the second equation is the same as equation (6), where $t_{hot} = T_{hot}/10^6$ K, is the temperature of the hot gas. Both equations can be solved for the filling factor ϵ, using the temperatures that correspond to our grid of hot gas models. The resulting filling factors range from 2×10^{-6} to 2×10^{-3}, and they are listed in the sixth column of Table 6.

Because of our assumption of spherical geometry for the hot phase, these estimates represent upper limits on the warm phase filling factors. Despite the large uncertainties the results suggest that the warm gas phase has a "clumpy" structure with many cool, dense cloudets.

5.4. *Where Does the Emission Spectrum Originate?*

Now that most of the relevant physical parameters have been constrained by the observed properties of the continuum, we need to check that they are also consistent with the emission-line spectrum. Unfortunately, this task is very difficult, as both gas phases might emit emission-line radiation. In particular, Williams et al. (1991) showed that gas at temperatures typical of the warm gas phase can emit high-ionization lines, which may also be found in a very hot gas. This, as a matter of fact, has been the main argument to question the presence of a "coronal line region" in novae in favor of a "coronal line stage." According to Williams, as the remnant's photosphere shrinks after the outburst, its temperature increases up to $\sim 10^6$ K, and the hardening of the radiation field would be capable of photoionizing the ejected gas to produce the observed coronal lines, while still having a low ($\sim 10^4$ K) temperature. This was confirmed by the model predictions for PW Vul's nebular shell given in Saizar et al. (1991). These showed that [Fe X] λ6374 was predicted to be strong in the nebular gas, although the warm gas did not produce the observed continuum.

To examine the relative contributions of each phase, we use our grid of models, to look at the predicted strengths of various emission lines. We have chosen some lines which can be expected to be strong in the hot gas. The infrared fluxes have been interpolated from the data given by Greenhouse et al. (1988). Using CLOUDY with the model parameters described

TABLE 7

EMISSION-LINE FLUXES IN THE HOT GAS

	$I_\lambda/I_{H\beta}$ (day 554)							
	Model Predictions							
T_{star} ($\times 10^6$ K) = 1.0 N_H ($\times 10^5$ cm^{-3}) = 0.2	1.0 0.3	1.0 0.5	0.5 0.6	0.5 0.8	0.5 1.4	0.2 2.0	0.3 3.0
LINE	Observed							
He II λ4686	0.5	...	...	...	0.1	0.2	0.7	3.0	5.1
N V λ1240	10.4	...	...	...	1.4	3.4	14.6	5.2	70.
Ne VI 7.6 μm	2.8	...	...	...	...	...	0.1	120.	150.
Mg VII λ2629	1.1	...	...	...	...	...	...	2.9	1.6
Mg VIII 3 μm	1.4	...	...	...	...	...	0.1	0.4	9.4
Si VI 2 μm	0.2	...	...	...	...	...	...	0.9	0.3
Si VII 2.5 μm	0.4	...	...	...	...	...	...	0.4	1.5
Si IX 3.9 μm	0.8	...	...	...	...	0.1	0.3	...	1.0

in the last section, we obtain the line intensities listed in Table 7. All lines have been normalized with respect to the observed intensity of Hβ for day 554.

The results suggest that the coldest models in our grid predict fluxes which are much stronger than observed, and thus, we can discard them as unlikely to be representative of the conditions in the hot gas phase. The other models show weaker lines as the temperature increases. However, as the warm gas might emit coronal emission, the fact that these lines are weak in some models does not rule them out.

The next step is to obtain a model of the shell that is consistent with both the high and low ionization lines. We will also compare our model with a simple one-phase "warm" shell, and the observed fluxes.

The models were obtained from the photoionization code CLOUDY, attached to an optimization routine that makes a non-parametric search for a best solution. The model parameters are listed in Table 8 and are defined as follows:

Model 1.—This is a one-phase high-density model which is photoionized by the white dwarf. The filling factor and the inner radius of the shell were varied to find a best solution. No significant improvement was found by varying the density with respect to the observed value.

Model 2.—The one-phase hot model. This solution is somewhat intermediate to the ones found in the grid above, and represents the best model found. Parameters were varied as before, but only the higher ionization lines were tried to fit.

Model 3.—This is also a warm-phase model, but this time the source of ionization is reprocessed (free-free and free-

TABLE 8

MODEL PARAMETERS

A.

Parameter	Model 1	Model 2	Model 3	Model 4
Ionizing Continuum	[a]	[a]	[b]	[a,b]
$T_*(10^4$ K)	30	30	N/A	30
$L_*(10^{38}$ ergs s^{-1})	2.0	2.0	2.0	2.0
$N_H(10^5$ cm^{-3})	100	1.0	100	1.0, 100
$R_{inner}(10^{14}$ cm)	7.0	10	10	10
$R_{outer}(10^{14}$ cm)	110	62	104	62,104
Filling factor	6.6×10^{-3}	1.0	1.0×10^{-2}	1.0, 1.0×10^{-2}

B.

ADOPTED ABUNDANCES[c]

Ratio	Value
He/H	5.0
C/H	0.8
N/H	44.0
O/H	10.0
Ne/H	60.0
Mg/H	6.0
Al/H	90.0
Si/H	2.0
Others	1.0

[a] Photoionization by a blackbody.
[b] Photoionization by free-free emission from the hot model.
[c] By number, relative to solar.

bound) radiation from the hot phase. The search was identical to Model 1, changing the input spectrum only.

Model 4.—A composite model. The predicted fluxes are simply the sums of Models 2 and 3.

We should stress here the fact that these are not necessarily the best possible models for QU Vul, as we have not explored the whole parameter space. In addition, other effects, such as the presence of dust, have also been neglected. These models, however, agree in general terms with the physical parameters obtained throughout this paper.

The predicted and observed intensities relative to Hβ are listed in Table 9. Each column is labeled after one of the models listed above. Note that Hβ is predicted to be significantly brighter than observed. Since observational errors can greatly affect individual lines, we have not attempted to also fit this particular line, which we only give as a reference.

The low- and intermediate-ionization lines are best explained by the single-phase warm model, although the composite model's predictions are not too far off, considering the uncertainties in the conditions of the hot gas. Let us define the quantity

$$\chi^2 = \sum \left(\frac{(O - M)}{M} \right)^2 , \qquad (10)$$

where O and M represent the observed and predicted fluxes relative to Hβ, respectively. For the low and intermediate ionization, Model 1 yields $\chi^2 = 6.9$, and Model 4, $\chi^2 = 45$. For the high-ionization lines, the values are 7,400 and 27, respectively. Including all lines, they are 7,400 and 72, respectively.

In conclusion, a model in which warm clumps are embedded in a hot tenuous environment can account reasonably well for the general characteristics of the observed ultraviolet/optical/infrared spectrum. However, more research needs to be done to investigate the effects of radial density variations, dust, and other ingredients, as well as to determine the chemical composition of the hot phase.

TABLE 9

MODELS FOR DAY 554[a]

Line	Model 1[b]	Model 3[c]	Model 4[d]	Observed
Hβ[e]	35.66	35.95	35.95	33.89
He I λ5876	0.53	0.48	0.48	0.24
He II λ1640	8.0	5.6	10.2	3.60
He II λ4686	0.85	0.60	1.1	0.51
C III] λ1909	0.97	0.49	0.49	0.90
C IV λ1549	5.1	2.8	3.5	1.90
[N II] λ5755	0.38	0.54	0.54	0.20
N III] λ1750	3.13	1.5	1.5	1.80
N IV] λ1486	6.3	3.3	3.3	5.40
N V λ1240	14.1	8.3	11.7	10.30
[O I] λ6300	0.12	0.02	0.02	0.10
[O II] λ7325	0.23	0.65	0.65	0.20
[O III] λ1660+1666	2.16	0.93	0.93	1.40
[O III] λ4363	2.29	1.2	1.2	1.50
[O III] λ4959+5007	7.83	5.4	5.4	6.50
O IV] λ1402	2.3	1.3	1.3	Blend
Si IV] λ1398	0.68	0.42	0.42	Blend
Total 1400	3.0	1.7	1.7	4.33
[Ne III] λ3869+3968	26.4	17.4	17.4	14.8
[Ne IV] λ1602	4.8	3.1	3.1	7.02
[Ne IV] λ4720	1.2	0.75	0.75	1.60
[Ne V] λ1575	1.1	0.66	0.66	1.20
[Ne V] λ3346	8.1	5.2	5.2	Blend
Ne III λ3343	0.18	0.1	0.1	Blend
Total 3346	8.3	5.3	5.3	11.89
Mg II λ2798	3.9	2.4	2.4	9.78
Al III λ1860	2.4	1.4	1.4	1.60
Si III] λ1892	0.45	0.27	0.27	1.00
[Fe VII] λ6087	0.07	0.05	0.05	0.10
High Ionization Lines				
[Ne VI] λ7.6 μm	0.66	0.39	2.33	2.8
[Mg VII] λ2629	0.31	0.18	0.54	1.1
[Mg VIII] λ3 μm	0.04	0.02	1.08	1.4
[Si VI] λ2 μm	0.14	0.09	0.1	0.2
[Si VII] λ2.5 μm	0.07	0.04	0.07	0.4
[Si IX] λ3.9 μm	0.00	0.00	0.28	0.8

[a] Entries give line fluxes with respect to *observed* H(β).
[b] Photoionization by a blackbody.
[c] Photoionization by free-free emission from a hot gas.
[d] Sum of warm (2) and hot (3) models.
[e] Entry is log L(Hβ).

5.5. *Energy Budget*

In the previous sections we have assumed that QU Vul maintained a luminosity equal to the Eddington level for a 1 $M_\odot$ star. Is this a reasonable assumption? From the visual light curve discussed in § 3, we found that the time to decline 2 mag was 25 days. From the luminosity–"speed class" relationship given by Warner (1989) we obtain an absolute magnitude at maximum, $M_V = -8.0 \pm 0.9$, which corresponds to a peak luminosity of 5.3×10^{38} ergs s^{-1}. This super-Eddington level has been observed in other novae (see, e.g., Starrfield 1989), and it is expected to be short-lived quickly reaching levels at or near the Eddington limit. The slow decline of the ultraviolet and optical light curves until day $\sim$500 (cf. S92) suggests that the integrated luminosity may have maintained a constant level during that period.

Let us assume that the white dwarf maintained a luminosity level equal to the Eddington limit for its mass, $L_{\rm Edd} \sim 2 \times 10^{38}$ ergs s^{-1}. At day 554, the total radiated energy was $\sim 10^{46}$ ergs. From the arguments above, this is clearly a lower limit to the emitted energy.

On the other hand, the kinetic energy of the shell (hot plus warm phases), is $1/2\, M_{\rm shell}\, v^2 \sim 5.6 \times 10^{44}$ and 2.5×10^{46} ergs, for the lowest and highest mass estimates just derived.

For a 1 $M_\odot$ white dwarf, and the ejected masses listed above, the liftoff energies required lie in the range 1.0×10^{46} to 5×10^{47} ergs. These numbers suggest that a significant fraction of the energy of the outburst is being carried by the hot gas phase.

6. SUMMARY AND DISCUSSION

The continuous spectrum of Nova QU Vul 1984 shows the signatures of a gas at high temperature: a nearly constant continuous flux (f_ν), extending from the ultraviolet into the infrared, and a nearly absent Balmer jump. The emission-line spectrum consisting of low- and medium-ionization species, on the other hand, indicates that they are originated in a much colder region. A model was then proposed in which the nova shell is composed of two distinct regions. The hot phase is photoionized by the postoutburst remnant, and the warm phase is photoionized by both the remnant and the hot phase.

These observations allowed us to constrain the electron temperature within the range $\sim 10^5$–10^6 K. These temperatures are well above the temperature of the warm phase ($\sim 10^4$ K),

derived in an earlier paper (S92), from nebular line diagnostics. We also set limits to the electron density, $N_e \sim 2 \times 10^4$ to 3×10^5 cm^{-3}. The hot gas is, therefore, two or three orders of magnitude more tenuous than the warm phase.

Using these results, we also found that the warm gas must be very clumpy, consisting of many cloudets only loosely associated to the hot gas (we do not find clear evidence of pressure equilibrium between the phases). The hot gas, however, is much more massive than its counterpart, and, although the exact geometry is not known, it seems reasonable to assume that it will not be as clumpy.

The high temperature in the hot shell makes it difficult for us to study its properties in detail. This difficulty is exacerbated by the fact that the warm phase can easily produce high-ionization lines, given the hard radiation field in which it is immersed. Photoionization modeling of this phase can, however, help us to examine its relative contribution to the high ionization emission. We then constructed a grid of models with parameters listed in Table 6. The results, shown in Table 7, lead us to believe that models with low ionization parameters (i.e., low T_e and high N_e), tend to overproduce the line fluxes as compared to observations. Not much can be said on the higher end of the temperature range, since little or no line emission is produced. However, our suspicion is that the best models lie about the center of our grid.

Next, we searched for a photoionization model of the shell that would be able to fit both the high and low ionization spectrum. We constructed two basic models: a simple one-phase, warm and clumpy shell, and a composite model in which the warm gas is embedded in a hotter, tenuous shell. In the first case, the warm gas is directly photoionized by radiation from the white dwarf, while in the second case, the star keeps the hot gas ionized, and reprocessed radiation from the latter, photoionizes the warm phase. In both cases, the parameters of the best models are consistent with those derived from the observations. However, we find that the composite model can fit reasonably well a larger range of ionization than the single-phase model.

The models seem to suggest that the white dwarf has a temperature of the order of 300,000 K, which is consistent with a study of QU Vul and other novae by Ögelman et al. (1987).

Finally, we also found that most of the ejected mass is contained within the hot phase, with a most likely ratio of hot to warm masses between 50 and 130 (see Table 6), which implies that the total ejected mass was in the range of 3 to 7×10^{-4} $M_\odot$. This is also consistent with an infrared study by Greenhouse et al. (1988).

The relatively large amount of gas returned to the interstellar medium by novae, in combination with their enhanced abundances, may have important implications for studies of galactic chemical enrichment. In S92, we estimated the contribution of QU Vul to the observed galactic aluminum, with the result that QU Vul, containing a low ONeMg white dwarf, should not be a very common kind of object. To our knowledge, only one other nova seems to resemble QU Vul: Nova Puppis 1991 (Saizar et al. 1994).

How do the returned mass of novae compare to supernovae? According to Weiler & Sramek (1988), the supernova rate is 2 ± 1 per century. This rate, however, includes all three accepted types of supernovae. Type Ia and Ib supernovae are estimated to lose 1 $M_\odot$ each in the explosion, while 5 $M_\odot$ are lost by Type II supernovae. The relative frequencies of Types Ia, Ib, and II are 3:4:11, respectively (Weiler & Sramek 1988). These figures imply that about 6.9 ± 3.5 $M_\odot$ are returned by galactic supernovae per century.

The return mass by novae is more difficult to calculate as very few mass determinations are available. For simplicity, we assume that each type of nova, C-O and O-Ne-Mg, have equal rate of occurrence, and ejected masses. Warner (1989) indicates that the rate of galactic novae of 100 per year may be an overestimate, and thus, his quote of 26 ± 4 per year corresponding to M31 may be a more realistic figure. In order to make an order-of-magnitude estimate, let us assume that the return mass by novae ranges between 10^{-4} $M_\odot$ and 4×10^{-3} $M_\odot$ per nova. Therefore, the total mass ejected by all novae ranges between 0.3 and 10 $M_\odot$ per century. This is comparable to the supernova rate, and, thus, novae should be taken into account in studies of chemical evolution.

We would like to thank the referee, M. Greenhouse, for several comments and suggestions that improved this paper. The support of NASA and NSF is also gratefully acknowledged.

APPENDIX

In § 5, we discussed and compared the results of different photoionization models of QU Vul's shell, using different assumptions concerning the nature of the ionizing source and physical state of the gas. In this appendix, we present additional results from our best models.

As before, we define our models as follows: "warm," a shell consisting of a single dense, warm phase, which is photoionized by the white dwarf; "hot," a single tenuous, hot gas, also photoionized by the white dwarf; and "composite," a composite model in which the white dwarf photoionizes the hot phase, and then processed radiation from the hot phase photoionizes the warm phase.

Electron Temperature.—The models predict that the average temperature in the O^{++} zone is 10,400 and 9520 K, for the warm and composite models. No O^{++} zone exists in the hot model. Both are in well agreement with the observed temperature of $10{,}000 \pm 800$ K.

Ion Abundances.—In Tables 10, 11, and 12 we list the average number density of each ionic species present in the model nebulae relative to hydrogen. The average is taken over the volume of the shell in each model.

TABLE 10

WARM-PHASE ION ABUNDANCES (MODEL 1)

	Ionization Stage[a]												
Ion	I	II	III	IV	V	VI	VII	VIII	IX	X	XI	XII	XIII
H	5.16(−1)	1.00											
He	5.71(−1)	6.97(−1)	2.48(−1)										
C	1.41(−3)	7.08(−1)	4.97(−1)	2.07(−1)	1.04(−1)	1.09(−4)							
N	4.78(−1)	2.44(−1)	4.70(−1)	1.68(−1)	7.21(−2)	8.57(−2)	3.96(−8)						
O	5.20(−1)	2.01(−1)	5.68(−1)	7.91(−2)	7.21(−2)	5.15(−2)	2.61(−2)						
Ne	3.10(−1)	3.18(−1)	6.37(−1)	7.43(−2)	1.18(−1)	5.46(−2)	4.39(−3)	7.96(−4)	1.36(−4)				
Mg	2.99(−3)	6.67(−1)	5.78(−1)	7.87(−2)	5.93(−2)	8.75(−2)	3.75(−2)	6.43(−3)	4.49(−4)	5.89(−6)			
Al	1.33(−3)	7.53(−1)	3.94(−1)	1.79(−1)	6.46(−2)	7.80(−2)	4.03(−2)	6.44(−3)	3.26(−4)	4.14(−6)			
Si	5.85(−4)	7.26(−1)	3.47(−1)	2.40(−1)	8.04(−2)	7.80(−2)	3.69(−2)	8.22(−3)	4.74(−4)	5.85(−6)			
S	7.87(−5)	6.31(−1)	5.13(−1)	1.81(−1)	3.76(−2)	7.48(−2)	7.41(−2)	6.59(−3)	2.68(−4)	2.47(−6)			
Ar	2.93(−1)	3.37(−1)	4.89(−1)	2.16(−1)	7.62(−2)	3.09(−2)	4.13(−2)	2.25(−2)	1.09(−2)	1.28(−5)			
Ca	3.85(−3)	1.46(−1)	1.06(+0)	9.02(−2)	2.07(−2)	5.45(−2)	7.14(−2)	4.44(−2)	1.95(−2)	3.42(−3)	4.19(−4)		
Fe	1.71(−2)	5.89(−1)	1.75(−1)	4.78(−1)	2.22(−2)	5.24(−2)	8.71(−2)	7.29(−2)	1.99(−2)	3.52(−3)	4.40(−4)	3.01(−5)	5.20(−7)

[a] Entries are number abundances relative to H^+.

TABLE 11

HOT-PHASE ION ABUNDANCES (MODEL 2)

	Ionization Stage[a]													
Ion	I	II	III	IV	V	VI	VII	VIII	IX	X	XI	XII	XIII	XIV
H	5.24(−8)	1.00												
He ...	0.00	7.89(−5)	1.00											
C	0.00	0.00	1.25(−5)	6.64(−3)	9.20(−1)	7.26(−2)	9.62(−5)							
N	0.00	0.00	0.00	1.09(−5)	4.00(−3)	9.95(−1)	9.59(−5)							
Ne ...	0.00	0.00	0.00	8.13(−8)	4.60(−4)	4.67(−2)	1.90(−1)	3.64(−1)	3.99(−1)					
Mg ...	0.00	0.00	0.00	0.00	1.60(−6)	1.06(−3)	6.53(−2)	4.52(−1)	4.28(−1)	5.32(−2)	1.44(−3)			
Al	0.00	0.00	0.00	0.00	2.05(−6)	1.16(−3)	8.59(−2)	5.05(−1)	3.60(−1)	4.80(−2)	7.87(−4)	3.18(−6)		
Si	0.00	0.00	0.00	0.00	1.53(−6)	8.83(−4)	5.61(−2)	4.78(−1)	4.10(−1)	5.41(−2)	1.30(−3)	2.52(−6)		
S	0.00	0.00	0.00	0.00	4.59(−6)	7.60(−4)	1.17(−1)	5.08(−1)	3.38(−1)	3.61(−2)	7.06(−4)	1.38(−6)		
Ar	0.00	0.00	0.00	0.00	0.00	4.09(−6)	8.30(−4)	3.90(−2)	9.35(−1)	2.39(−2)	2.04(−4)	1.69(−7)		
Ca ...	0.00	0.00	0.00	0.00	0.00	0.00	1.44(−5)	2.36(−3)	7.91(−2)	3.79(−1)	5.40(−1)	1.88(−5)		
Fe	0.00	0.00	0.00	0.00	0.00	0.00	1.15(−5)	3.52(−3)	8.83(−2)	3.32(−1)	3.80(−1)	1.66(−1)	2.78(−2)	2.27(−3)

[a] Entries are number abundances relative to H^+.

TABLE 12

EMBEDDED WARM-PHASE ION ABUNDANCES (MODEL 3)

	Ionization Stage[a]												
Ion	I	II	III	IV	V	VI	VII	VIII	IX	X	XI	XII	XIII
H	1.52(−2)	1.00											
He	2.17(−1)	6.22(−1)	1.77(−1)										
C	6.76(−4)	2.81(−1)	5.10(−1)	1.43(−1)	8.13(−2)	6.95(−5)							
N	1.15(−2)	3.08(−1)	4.66(−2)	1.15(−1)	5.46(−2)	6.22(−2)							
O	1.52(−2)	3.24(−1)	5.10(−1)	5.62(−2)	5.47(−2)	3.85(−2)	1.76(−2)						
Ne	2.61(−2)	3.02(−1)	5.14(−1)	5.36(−2)	8.34(−2)	3.40(−2)	2.69(−3)	4.09(−4)					
Mg	1.82(−4)	1.43(−1)	6.90(−1)	5.86(−2)	4.43(−2)	5.42(−2)	2.26(−2)	4.01(−3)	2.21(−4)	1.63(−6)			
Al	8.11(−1)	2.70(−1)	4.53(−1)	1.71(−1)	4.75(−2)	4.68(−2)	2.41(−2)	4.03(−3)	1.57(−4)	1.10(−6)			
Si	2.37(−5)	1.77(−1)	4.70(−1)	2.24(−1)	6.82(−2)	4.84(−2)	2.24(−2)	5.20(−3)	2.42(−4)	1.71(−6)			
S	3.48(−6)	1.92(−1)	5.19(−1)	1.63(−1)	2.72(−2)	5.36(−2)	5.68(−2)	4.49(−3)	1.31(−4)	6.25(−7)			
Ar	6.15(−3)	2.47(−1)	4.46(−1)	1.82(−1)	5.58(−2)	2.29(−2)	3.36(−2)	1.56(−2)	7.33(−3)	6.58(−6)			
Ca	1.30(−4)	3.52(−3)	8.03(−1)	5.70(−2)	1.58(−2)	4.35(−2)	5.09(−2)	2.74(−2)	1.29(−2)	2.11(−3)	1.85(−4)		
Fe	8.61(−4)	7.45(−2)	3.04(−1)	4.57(−1)	1.40(−2)	4.30(−2)	6.40(−2)	4.37(−2)	1.32(−2)	2.24(−3)	2.06(−4)	7.08(−6)	6.05(−8)

[a] Entries are number abundances relative to H^+.

REFERENCES

Bath, G. T., & Shaviv, G. 1976, MNRAS, 175, 305
Davidson, K. 1977, ApJ, 218, 20
Ferland, G. J. 1080, PASP, 92, 596 (F80)
———. 1993, Univ. of Kentucky Astronomy Department Internal Report
Ferland, G. J., Lambert, D. L., & Woodman, J. H. 1977, ApJ, 213, 132
———. 1986, ApJS, 60, 375
Gallagher, J. S., & Ney, E. 1976, ApJ, 204, L35
Gallagher, J. S., & Starrfield, S. 1976, MNRAS, 176, 53
Grasdalen, G., & Joyce, R. R. 1976, Nature, 259, 187
Greenhouse, M. A., Grasdalen, G. L., Hayward, T. L., Gehrz, R. D., & Jones, T. J. 1988, AJ, 95, 172
Ögelman, H., Krautter, J., & Beuermann, K. 1987, A&A, 177, 110
Osterbrock, D. E. 1989, Astrophysics of Gaseous Nebulae and Active Galactic Nuclei (Mill Valley, CA: University Science)
Saizar, P., et al. 1991, ApJ, 367, 310
———. 1992, ApJ, 398, 651 (S92)
Saizar, P., et al. 1994, in preparation
Seaton, M. J. 1978, MNRAS, 185, 5P
Shields, G. A., & Ferland, G. J. 1978, ApJ, 225, 950
Starrfield, S. 1989, in Classical Novae, ed. A. Evans & M. Bode (New York: Wiley), 123
———. 1990, in Evolution in Astrophysics, ed. E. Rolfe (ESA SP-310) (Noordwijk: ESA), 101
Starrfield, S., Sparks, W. M., & Truran, J. W. 1986, ApJ, 303, L5
Taylor, A. R., Seaquist, E. R., Hollis, J. M., & Pottasch, S. R. 1987, A&A, 183, 38
Warner, B. 1989, in Classical Novae, ed. N. Evans & M. Bode (New York: Wiley), 1
Weiler, K. W., & Sramek, R. A. 1988, ARA&A, 26, 295
Williams, R. E. 1992, ApJ, 392, 99
Williams, R. E., Hamuy, M., Phillips, M. M., Heathcote, S. R., Wells, L., & Navarrete, M. 1991, ApJ, 376, 721